PART 2: Continuous spectrum from the solar atmosphere

Maren Rasmussen [1]

https://github.com/mjauren/AST4310

[1] Institute of Theoretical Astrophysics, P.O. Box 1029, Blindern, N–0315 Oslo, Norway

Abstract. This report contains a study of the solar continuum at visible and infrared wavelengths assuming H^- as the main provider of the extinction, using data from Allen (1973) and Foneta et al. (1993). We have found a correlation between the brightness temperature and the depth in the surface where the extinction is emitted. We have also found that the H^- extinction per cm decreases exponentially outwards through the atmosphere, and that the intensity from wavelength $\lambda = 1.6\,\mu$m is emitted deepest in the solar atmosphere. Using computed values for the mean height of formation, the height where the optical thickness is equal to 1, and the height where the brightness temperature equals the actual temperature, we have seen that the local thermodynamical equilibrium Eddington-Barbier approximation holds in the atmosphere. And in the end we found that the sun has a clear limb darkening due to the decrease in temperature further out in the photosphere.

1. Introduction

It is highly recommended to read through Part 1 found further down in this article before reading this part. Part 1 will give you a better insight in the solar atmosphere and therefore give you a good foundation to understand this part better.

Stellar spectra can provide a lot of information about the conditions in stars, and our own Sun, and has been studied for many years. In this report we will study the continuous spectrum from the solar atmosphere using data from Allen (1973). Continuous spectra is formed by continuous extinction and emission. Usually we talk about four different global types of continuous radiative processes. The first one is extinction and emission as a result of the acceleration charged particles in electric fields. The next one is extinction and emission as result of the acceleration of charged particles in magnetic fields. Both these two processes follows from Maxwell's equations, which says that an electric charged particle experiencing acceleration, will emit electromagnetic radiation. The last two processes is extinction and emission from nuclear reactions, and effects from collective electric fields (Rutten (1991)).

Through the report we will mainly focus on data from visible and near-infrared wavelengths. The data from Allen (1973) gives us the measured radially emergent intensity and the astrophysical flux in the solar continuum with and without smoothed lines for wavelengths between 0.2 and 5 μm. We will assume that H^- is the major provider of continuous extinction, which is a good assumption for the solar photosphere for wavelengths $\lambda > 0.5\,\mu$m. We will also assume local thermodynamical equilibrium. We will also use some data from Foneta et al. (1993) giving parameters describing the solar atmosphere and the average parameters in the Earths atmosphere. The first section in the report will give a introduction in the expressions and quantities used to obtain the results. Thereafter we will shortly present the method. Then the results will be presented. And the report will end with a conclusion.

The codes used in this project is written in `Python 3.6.6` and can be found on my GitHub page located beneath the my name under the title. Here a description of the programs can also be found.

2. Theory

2.1. Radially emergent intensity and astrophysical flux

As mentioned in the introduction, the data from Allen (1973) gives us the measured radially emergent intensity and the astrophysical flux in the solar continuum with and without smoothed lines. Spectra from the sun will always contain a lot of absorption and extinction lines with small amplitudes, these can be filtered away by smoothing the spectra. Smoothing the spectra will also make it easier to extract the main spectral lines we often are interested in.

Astrophysical flux is defined as

$$\pi F_\lambda \equiv \mathcal{F}_\lambda \tag{1}$$

where $\mathcal{F}$ is the net outward flow of energy through a stellar surface element. By multiplying the net outward flux with π, we get a flux measured per steradian. Therefore will all these spectral distributions have the same unit, [erg cm^{-2} s^{-1} μm^{-1} ster^{-1}]. The difference between the astrophysical flux and the intensity, is that the astrophysical flux gives the average intensity over the stellar disk received by a distant observer, $F_\lambda = \langle I_\lambda \rangle$.

2.2. Spectral bandwidth

The radially emergent intensity and the astrophysical flux used in this report is given per wavelength bandwidth $\Delta\lambda = 1\,\mu$m. Often it is interesting to study how these quantities change when they instead are studied per frequency bandwidth $\Delta\nu = 1$ Hz. It can be derived that

$$I_\nu = \frac{c}{\nu^2} I_\lambda \Rightarrow I_\nu = \frac{\lambda^2}{c} I_\lambda, \tag{2}$$

where I_ν is the intensity given per frequency bandwidth, c is the speed of light, $\nu = c/\lambda$ is the frequency and λ is the wavelength. The same relation holds for the astronomical flux

$$F_\nu = \frac{\lambda^2}{c} F_\lambda. \tag{3}$$

Here F_ν is the flux given per frequency bandwidth.

2.3. Planck's function

Planck's function gives the radiation intensity emitted by a perfect blackbody with a certain temperature. This intensity is given by

$$B_\lambda(T) = \frac{2hc^2}{\lambda^5}\frac{1}{e^{hc/\lambda kT} - 1}, \tag{4}$$

where h is the Planck constant, c is the speed of light, k is the Boltzmann constant, λ is the wavelength and T is the temperature.

The brightness temperature T_b is the temperature that reproduces the observed intensity at a particular wavelength when it is inserted in the Planck function. In other words, if we insert the brightness temperature in the Planck function, we will get the observed intensity, $B_\lambda(T_b) = I_\lambda^{\text{obs}}$. This means that by inverting Planck's law, we can get an expression for the brightness temperature T_b,

$$\begin{aligned} B_\lambda(T_b) = I_\lambda &= \frac{2hc^2}{\lambda^5}\frac{1}{e^{hc/\lambda kT_b} - 1} \\ \frac{I_\lambda\lambda^5}{2hc^2} &= \frac{1}{e^{hc/\lambda kT_b} - 1} \\ \frac{2hc^2}{I_\lambda\lambda^5} &= e^{hc/\lambda kT_b} - 1 \\ \frac{hc}{\lambda kT_b} &= \ln\left(\frac{2hc^2}{I_\lambda\lambda^5}\right) + 1 \\ T_b &= \frac{hc}{\lambda k \ln\left(\frac{2hc^2}{I_\lambda\lambda^5}\right)}. \end{aligned} \tag{5}$$

2.4. Optical depth

Optical depth is a measure on how transparent a material is for photons travelling through it. The optical depth is given by

$$\tau_\lambda(h_0) \equiv -\int_\infty^{h_0} \alpha_\lambda^c dh \tag{6}$$

where h_0 is any height and α_λ^c is the continuous extinction.

2.5. Emergent intensity

By assuming plane-parallel stratification, the radiation emerging from the center of the solar disk can be given by

$$I_\lambda = \int_0^\infty S_\lambda e^{-\tau_\lambda} d\tau_\lambda$$

where S_λ is the source function which we in thermodynamical equilibrium can assume to be equal to the Planck function. This expression can also be rewritten to give the intensity that emerges under an angle $\mu = \cos\theta$ in a plane-parallel approximation,

$$I_\lambda(0,\mu) = \int_0^\infty S_\lambda e^{-\tau_\lambda/\mu} d\tau_\lambda/\mu. \tag{7}$$

The radius of the apparent solar disk is given by

$$r/R_\odot = \sin\theta,$$

where $\sin\theta$ is given by

$$\begin{aligned} \mu &= \cos\theta \\ \cos^{-1}\mu &= \theta \\ \sin\theta &= \sin(\cos^{-1}\mu) = \sqrt{1-\mu^2}. \end{aligned}$$

Another interesting quantity is the intensity contribution function which gives the contribution of each layer to the emergent intensity. The contribution is given by

$$\frac{dI_\lambda}{dh} = S_\lambda e^{-\tau_\lambda}\alpha_\lambda. \tag{8}$$

Its weighted mean defines what we call the mean height formation, and is given by

$$\langle h\rangle \equiv \frac{\int_0^\infty h(dI_\lambda/dh)dh}{\int_0^\infty (dI_\lambda/dh)dh} = \frac{\int_0^\infty hS_\lambda e^{-\tau_\lambda}d\tau_\lambda}{\int_0^\infty S_\lambda e^{-\tau_\lambda}d\tau_\lambda} \tag{9}$$

2.6. The Eddington-Barbier approximation

The Eddington-Barbier approximation says that the emergent intensity I_λ for $\mu = 1$ is equal to the source function S_λ where the optical depth is equal to one, $\tau_\lambda = 1$. Written in another way, the Eddington-Barbier approximation reads

$$I_\lambda \approx B_\lambda(T[\tau_\lambda = 1]) \tag{10}$$

where we have used that $S_\lambda = B_\lambda$ in local thermodynamical equilibrium.

2.7. Emergent astrophysical flux

The emergent astrophysical flux can be found be integrating the intensity over emergence angle,

$$F_\lambda(0) = 2\int_0^1 I_\lambda(0,\mu)\mu d\mu. \tag{11}$$

But note here that equation 7 cannot be evaluated for $\mu = 0$. Therefore we instead cam evaluate the integration using "open quadrature", which is an integration formula neglecting the endpoints. The Gaussian quadrature is one of several quadrature formulas, given by

$$\int_{-1}^{+1} f(x)dx \approx \sum_{i=1}^{n} w_i f(x_i),$$

where the required abscissa values x_i and the weights w_i are tabulated for $n = 2 - 10$ and some higher orders on page 916 in Abramowitz & Stegun (1964). More about Gaussian quadrature can be found in Press et al. (1986). For our purpose, it is sufficiently to use three-point Gaussian integration to reach a good enough accuracy.

3. Method

All the plots in this report is made using simple implementations of the functions presented in section 2 in `Python 3.6.6`. The code making each plot is made as functions which can be called with and without a boolean parameter called `save`. If this parameter is true, the plot will be saved as an PDF-file. The functions are mainly named after which section they belong to in the assignment explaination in Rutten (1991). As mentioned earlier, all code can be found in the GitHub link provided under my name on the front page.

4. Results and discussion

4.1. Observed solar continua

Figure 1 shows the solar spectra distribution plotted with respect to wavelength at the solar surface. It shows both the radially emergent intensity I_λ and the astrophysical flux F_λ in the solar continuum with and without smoothed lines. The primed intensity and flux marks the smoothed lines.

The maximum value of I'_λ is 4.6 [erg cm^{-2} s^{-1} μm^{-1} ster^{-1}], this value is reached at wavelength $\lambda = 0.41$ μm. This means that most intense light from the sun is emitted in the visible spectre close to ultra violet light. We can also see this from the figure.

By using the relations given in equation 2 and 3 we can plot I_ν and F_ν with respect to the wavelength as done in figure 2. The maximum value of I'_ν is $4.21 \cdot 10^{-5}$ [erg cm^{-2} s^{-1} ster^{-1} Hz^{-1}], this value is reached at wavelength $\lambda = 0.80$ μm. We can also see this from the figure.

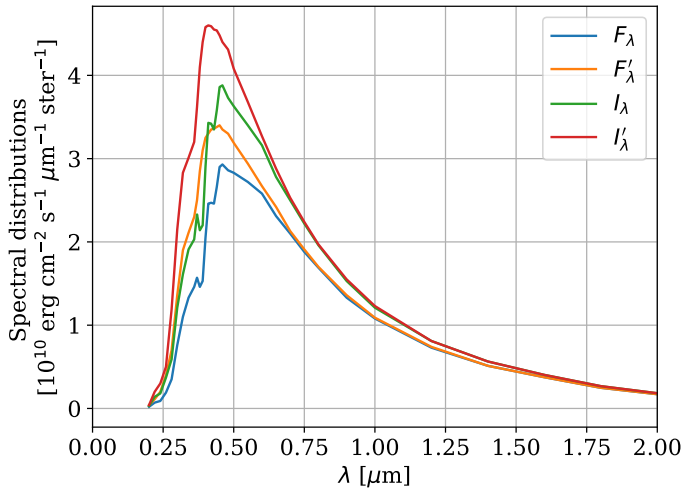

Fig. 1: Astrophysical flux F_λ and radially emergent intensity I_λ in the solar continuum, plotted with respect to wavelength λ, with and without smoothed lines. The primed intensity and flux marks the smoothed lines.

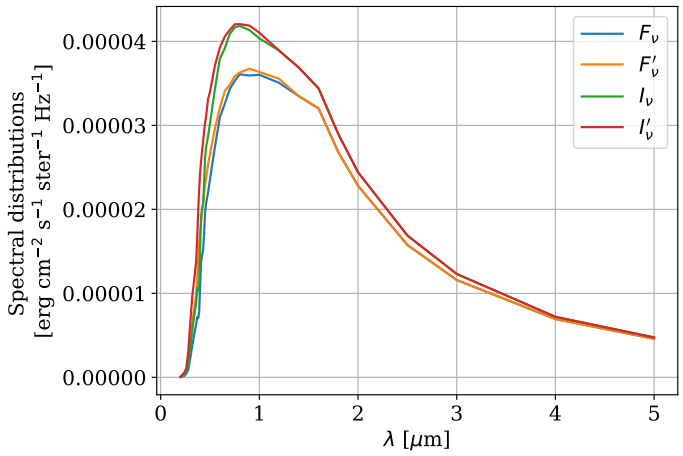

Fig. 2: Astrophysical flux F_ν and radially emergent intensity I_ν in the solar continuum, plotted with respect to wavelength λ, with and without smoothed lines. The primed intensity and flux marks the smoothed lines.

By plotting the Planck's law given in equation 4 for the same wavelengths as the previous plots using different temperatures, we can try to fit the function to the intensity I'_λ. This is done in figure 3 where we can see that for $T = 6500$ K, Planck's law fits best. This means that if the Sun had been a perfect blackbody, it would have a temperature of around 6500 K. The peak is only a bit higher from Planck's law, so the actual temperature might be a bit lower than 6500 K.

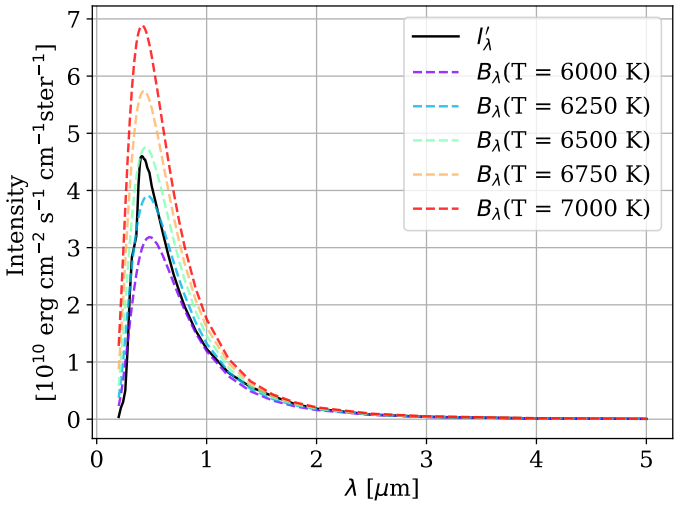

Fig. 3: Planck's law for different temperatures plotted together with radially emergent intensity I_λ for smoothed spectral lines, with respect to wavelength λ. B_λ(T=6500 K) fits best.

The brightness temperature from equation 5 is plotted with respect to wavelength in figure 4, where we can see that it peaks at $\lambda = 1.6$ μm with a maximum value of 6711 K. This means that where we have the highest brightness temperature, we will have radiation with wavelength around 1.6 μm, which corresponds to near infrared light. That this is where we have the highest brightness temperature, also implies that it is here we look most deep into the sun, because the extinction is larger deeper in the atmosphere. We can also see a peak around 0.4 μm, corresponding to violet light, with temperature 6500 K. Between these two peaks we have a valley at $\lambda \approx 1$. This means that the light with this wavelength is emitted a bit higher in the atmosphere, as it has a lower extinction.

4.2. Continuous extinction

Figure 5 shows the H$^-$ extinction per cm^2 per neutral hydrogen from the solar surface, with parameters taken from the FALC data file. We can compare our figure with the figure found on page 140 in Gray (1992), and see several similarities. The total extinction in Gray's figure also includes the extinction from neutral H, which causes it to have some peaks we do not have in our figure. The reason why we do not see bound free edges in the plot for H$^-$, as we would see for neural hydrogen, is that H^- is not hydrogenic because it has two bound electrons. The two electrons has to have a high correlation in motion and position for the three-body system to be stable, because hydrogen usually are neutral and "do not want" any more electrons. Therefore the H^- atoms cannot be excited.

By plotting the inverse of the extinction (extinction to the power of negative 1) we get a plot more similar to the plot we got of the brightness temperature in figure 4. The reason for this

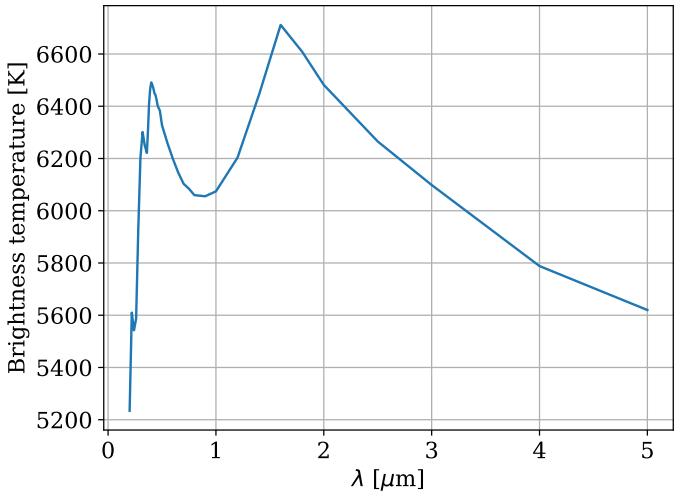

Fig. 4: Brightness temperature T_e plotted with respect to the wavelength.

is that where we have less extinction, the brightness temperature is larger.

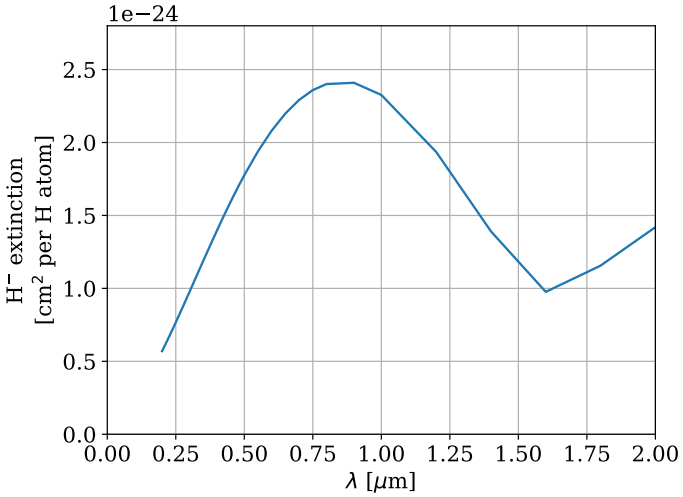

Fig. 5: The H^- extinction from the solar surface plotted with respect to the wavelength λ.

Figure 7 shows the H^- extinction per cm, Thomson scattering of free electrons per cm and the total extinction per cm, all plotted with respect to height at $\lambda = 0.4$ μm. It is plotted with a logarithmic y-axis because as we move higher up in the atmosphere, the optically thickness falls off roughly exponentially, which means that the extinction also falls off steeply (Rutten (1991)). The Thomson cross section per electron is $^T = 6.648 \cdot 10^{-25}$ cm^2. So the extinction is obtained by multiplying with the electron number density n_e. We can see from the plot that H^- extinction dominates at heights lower than around 1000 km, and higher than this height, the Thomson scattering of electrons starts dominating. This is because the number density of hydrogen is highest at lower heights, and decreases with height. The electron number density also have a somewhat decrease with height, but becomes more stable higher up in the atmosphere than 1000 km.

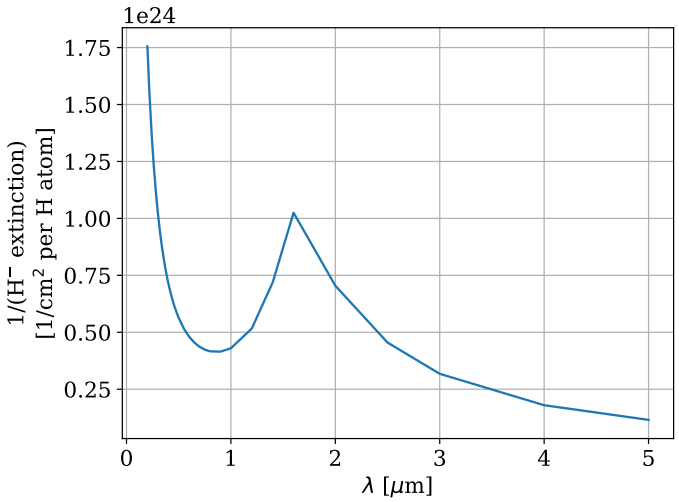

Fig. 6: The $(H^-$ extinction$)^{-1}$ from the solar surface plotted with respect to the wavelength λ.

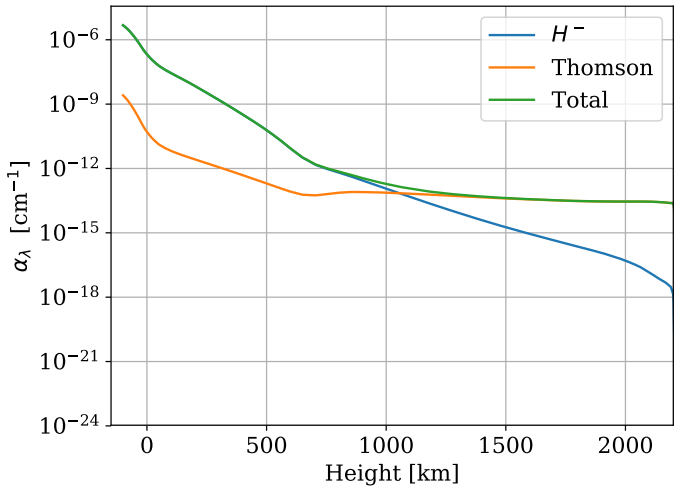

Fig. 7: H^- extinction per cm, Thomson scattering of free electrons per cm and the total extinction per cm plotted with respect to height for wavelength $\lambda = 0.4$ μm.

4.3. Optical depth

By integrating equation 6 at $\lambda = 500$ nm, we obtain the τ_{500} scale shown in figure 8. Here the optical depth gotten from the FALC datafile is also shown. We can see that the two are very similar.

4.4. Emergent intensity and height of formation

Figure 9 shows the peak normalized contribution function given in equation 8 plotted with respect to height for different wavelengths. The plot also shows the mean height of formation from equation9 for the different wavelengths.

From the mean height of formations, we can again (as we concluded in section 4.1) conclude that for $\lambda = 1.6$ μm, the average of the emergent intensity is emitted deepest in the atmosphere with $\langle h \rangle = -17.9$ km. We can also see that the contribution function peaks at the lowest height compared to for the other wavelengths, which means that most of the contribution to radiation with $\lambda = 1.6$ μm is emitted at this height. For $\mu = 1$

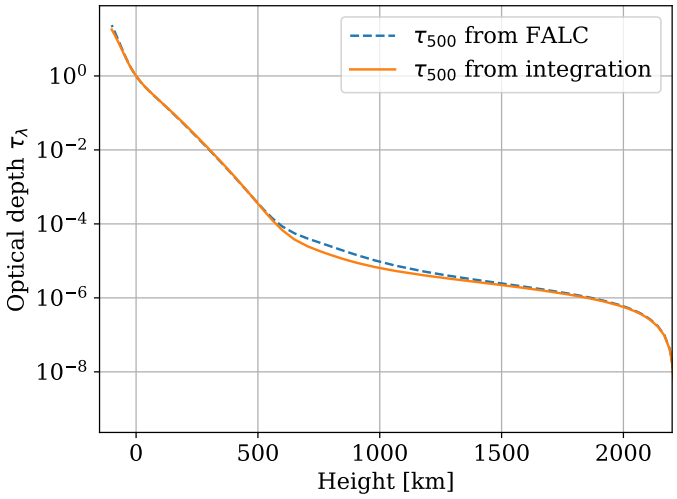

Fig. 8: Optical depth at $\lambda = 500$ nm both obtained from the FALC datafile and from equation 6 plotted with respect to height.

we know from figure 4 that the light is emitted higher up in the atmosphere. We see the same result from the mean height of formation $\langle h \rangle = 24.1$ km given in this figure. And again from figure 4 we know that light with wavelength $\lambda = 0.5$ μm is again emitted deeper in the atmosphere with a mean height of formation of $\langle h \rangle = -3.1$ km. And at last, the longest wavelength $\lambda = 5$ μm clearly gives emitted light highest up in the atmosphere.

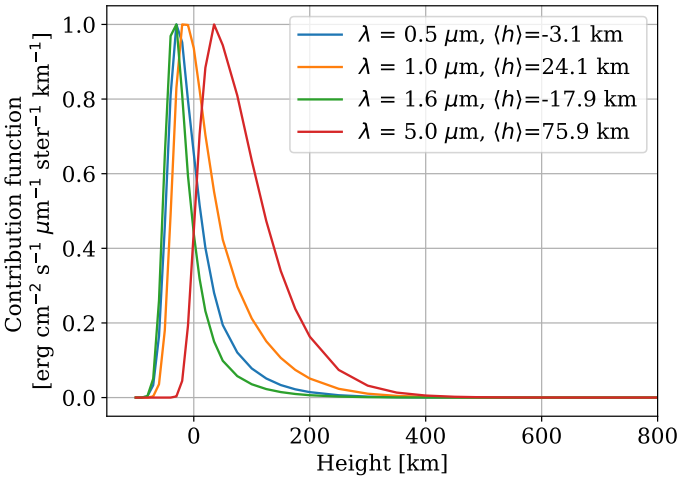

Fig. 9: Peak normalized contribution function plotted with respect to height for $\lambda = 0.5\mu$m, $\lambda = 1.0\mu$m, $\lambda = 1.6\mu$m and $\lambda = 5.0\mu$m. The mean height of formation is also given.

In table 1 we have compared the values of the mean height of formation $\langle h \rangle$, the height in the atmosphere where $\tau_\lambda = 1$ and the height where the temperature is equal to the brightness temperature for different wavelengths to check the validity of the local thermodynamical equilibrium Eddington-Barbier approximation given in equation 10. The heights in the atmosphere where $\tau_\lambda = 1$ is found by making figures similar to figure 8 for the different wavelengths. And the heights the temperature is equal to the brightness temperature is found by looking at both the brightness temperature plot in figure 4 and the plot showing the temperature plotted with respect to the height in figure 1. From the table we can see that the heights differs with a few kilometers, but compared the the height of the hole solar atmosphere, this is not much. So we can assume that the Eddington-Barbier approximation holds.

Table 1: Validation check of the Eddington-Barbier approximation.

λ	$\langle h \rangle$	$h(\tau = 1)$	$h_{T_b = T(h)}$
0.5 μm	-3.1 km	0 km	10 km
1.0 μm	24.1 km	13 km	28 km
1.6 μm	-17.9 km	-26 km	-10 km
5.0 μm	75.9 km	58 km	70 km

4.5. Disk-center intensity

By computing the intensity contributions as given in figure 9 for all wavelengths, we can obtain a full intensity graph for the solar atmosphere. The result of doing this is shown in figure 10. Here we can see that the computed solar continuum is very is very similar to the observed solar continuum, especially for larger wavelengths. For shorter wavelengths the computed intensity is somewhat too high.

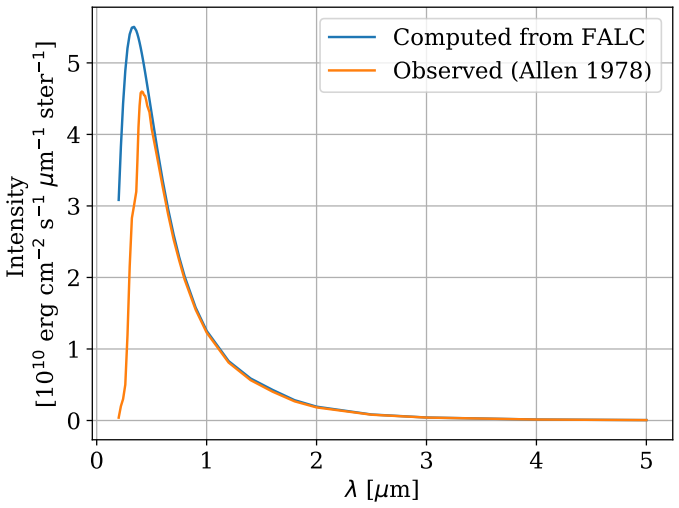

Fig. 10: Computed and observed solar continuum plotted with respect to wavelength. They are very similar for long wavelengths, but the computed continuum is somewhat off for shorter wavelengths.

4.6. Limb darkening

Figure 11 and figure 12 shows the computed ratio $I_\lambda(0, \mu)/I_\lambda(0, 1)$ plotted with respect to angle $\mu = \cos\theta$ and radius of the apparent solar disk $r/R_\odot = \sin\theta$ respectively. We can see from the plots that as we move further out on the solar disk, the intensity ratio decreases. We can also see that it increases faster for for shorter wavelengths. The reason why we see this limb darkening, is that the temperature decreases towards the outer layers of the photosphere, and therefore $S_\lambda(h) = B_\lambda[T(h)]$ also decreases outwards. This means that the intensity given by equation 7 decreases, and we get this darkening.

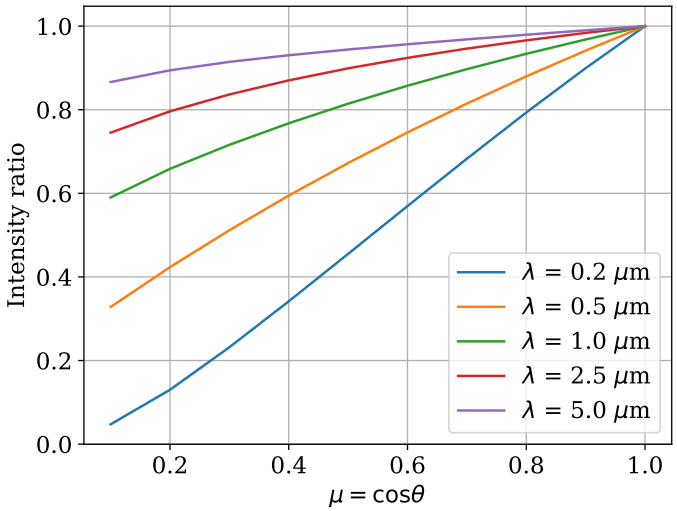

Fig. 11: The computed ratio $I_\lambda(0,\mu)/I_\lambda(0,1)$, where $I_\lambda(0,\mu)$ is given by equation 7, plotted with respect to angle $\mu = \cos\theta$.

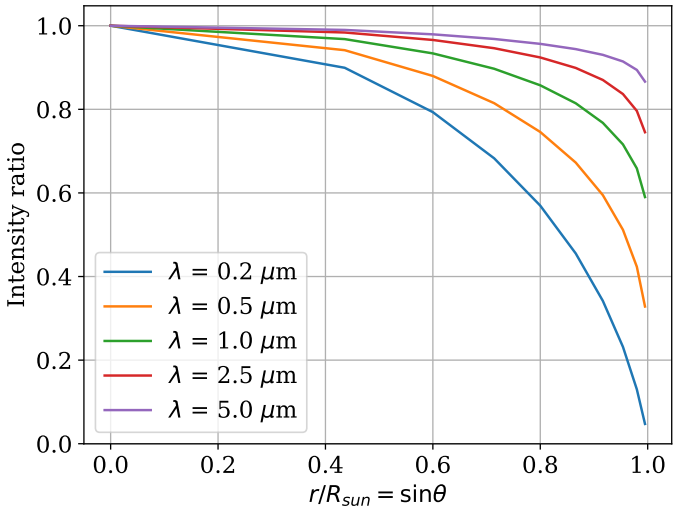

Fig. 12: The computed ratio $I_\lambda(0,\mu)/I_\lambda(0,1)$, where $I_\lambda(0,\mu)$ is given by equation 7, plotted with respect to the radius of the apparent solar disk $r/R_\odot = \sin\theta$.

4.7. Flux integration

The emergent solar flux can be found by evaluating equation 11 using Gaussian quadrature as written in section 2.7, and the result is shown in figure 13. Similar to figure 10 where we compared the computed emergent intensity to the observed intensity, we can that the computed and observed emergent astrophysical flux differ a bit for small wavelengths, but are very similar for larger wavelengths.

5. Conclusions

Through this report we have used data from Allen (1973) and Foneta et al. (1993) to study the solar continuum at visible and infrared wavelengths with H^- as the main provider of the extinction. We have found that there is a correlation between the $H^\cdot$ extinction and the brightness temperature in the solar atmosphere, giving that a higher brightness temperature for a given

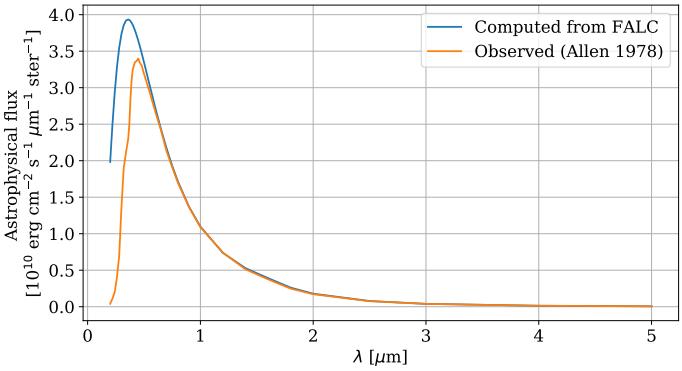

Fig. 13: The observed and computed emergent solar flux plotted with respect to wavelength.

wavelength, means that this wavelength is emitted deeper in the atmosphere. We have also found that the H^- extinction per cm decreases exponentially outwards through the atmosphere, and that the intensity from wavelength $\lambda = 1.6\,\mu$m is emitted deepest in the solar atmosphere.

Further we have compared numerically calculated values with observed values for the optical depth, emergent intensity and emergent flux, and found quite good similarities. We have also used the mean height of formation, the height where the optical thickness is equal to 1, and the height where the brightness temperature equals the actual temperature to find that the local thermodynamical equilibrium Eddington-Barbier approximation holds. In the end we found that the sun has a clear limb darkening due to the decrease in temperature further out in the photosphere.

References

Abramowitz, M. & Stegun, I. A., eds. 1964, Handbook of Mathematical Functions, Applied Mathematics Series 55 (Washington, DC: NBS)
Allen, C. W. 1973, Astrophysical quantities
Foneta, J., Avrett, E. H., & Loeser, R. 1993, Astrophys J.
Gray, D. F. 1992, The observation and analysis of stellar photospheres, 2nd edn. (Cambridge ; New York : Cambridge University Press)
Press, W. H., Flannery, B. P., Teukolsky, S. A., & Vetterling, W. T. 1986, Numerical Recipes
Rutten, R. J. 1991, Introduction to astrophysical radiative transfer

PART 1

1. Introduction

In this part of the report we will study the radial stratification of the solar atmosphere using data from Foneta et al. (1993), to get a good foundation when moving on to part 2. We will assume that the solar atmosphere is horizontally homogeneous or have "plane parallel layers" and that it is in hydrostatic equilibrium which means that it is time independent. The FALC model from Foneta et al. (1993) gives data at different heights in the atmosphere, where $h = 0$ is the point where the optical depth $\tau_{500} = 1$ at wavelength $\lambda = 500$ nm. The data gives observations og the column mass m, the temperature T, the microturbulent velocity v_t, the number density of hydrogen n_H, protons h_p and electrons n_e, the total pressure and the ratio between the gas pressure and the total pressure $P_{\text{gas}}/P_{\text{tot}}$ and, in the end, the density ρ.

This part of the report will not contain sections as in part 2, but will rather contain only a "Results" section with figures with more detailed captions.

2. Results

2.1. The solar atmosphere

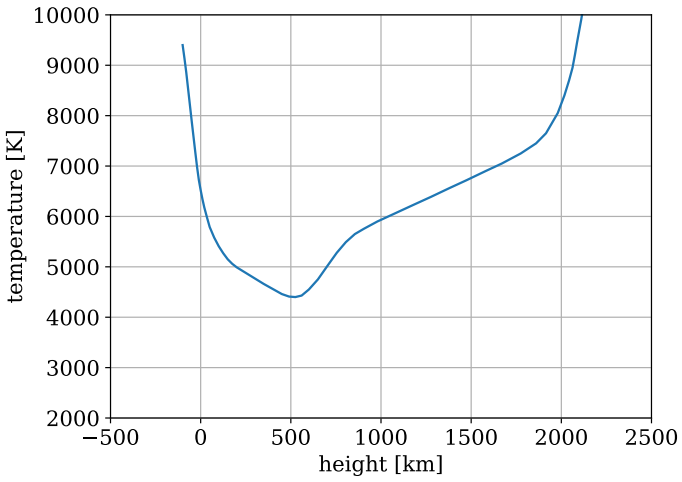

Fig. 1: The temperature plotted with respect to the height in the solar atmosphere. We can see that in the photosphere, at $-100 \leq h \leq 525$ km, the temperature is decreasing to a minimum of around 5500 K at 500 km. Thereafter, when we move into the chromosphere of the sun, at $525h \leq 2100$ km, the temperature is slightly increasing until a height of around 2000 km, where the temperature suddenly has a rapidly increase. This region from 2100 km and higher up in the atmosphere is called the transition region.

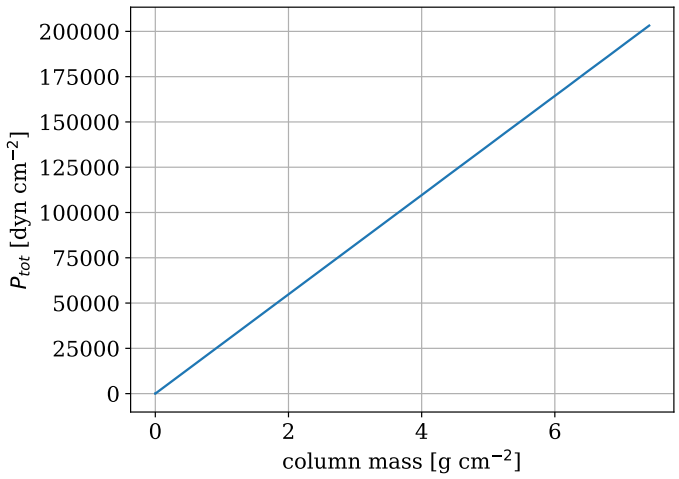

Fig. 2: The total pressure plotted with respect to the column mass. We can see that they scale linearly.

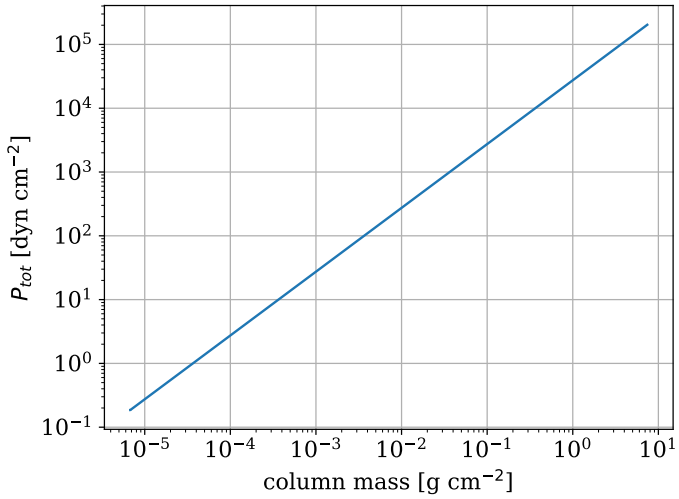

Fig. 3: The total pressure plotted with respect to the column mass with logarithmic axis. Again we can see that they scale linearly. Therefore we can conclude that $p_{total} = cm$ where c is the slope of the graph. Physically c is the solar surface gravity. By either finding the slope of the graph or calculating $c = p_{total}/m$, we get that $c \approx 27398$. cm/s^2.

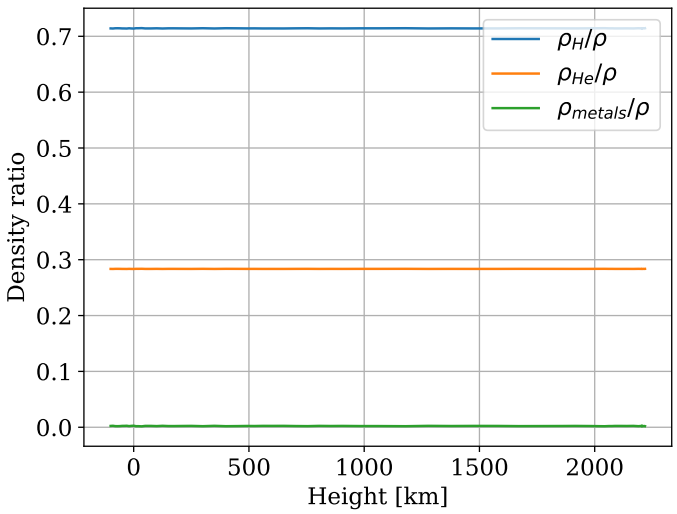

Fig. 4: The density ratios of the hydrogen mass density (blue line), helium mass density (orange line) and metal mass density (green line) to the total mass density, plotted against height. We can see that hydrogen clearly contributes most to the density, and that the metals does almost not contribute at all. They all seem quite constant, but there is some small perturbations.

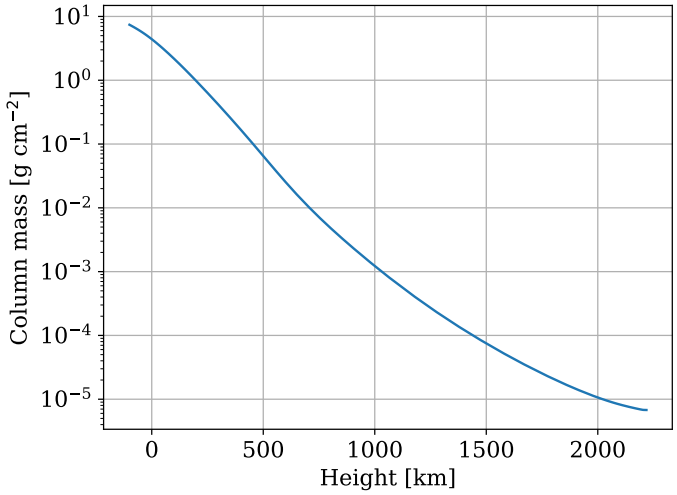

Fig. 5: The column mass plotted with respect to the height with logarithmic y-axis. We can see that the column mass is nearly linearly decreasing with height, but it is not exactly straight. The linear decrease tells us that the column mass is nearly logarithmic increasing as we move deeper into the atmosphere of the Sun. From figure 2 and 3 we know that as the pressure increases, the column mass increases as well. We also know that the pressure is higher deeper in the atmosphere, and therefore the column mass must increase deeper in the atmosphere as well. The reason to why the graph flattens out in the outer layers of the atmosphere might have something to do with the high temperatures and low pressure.

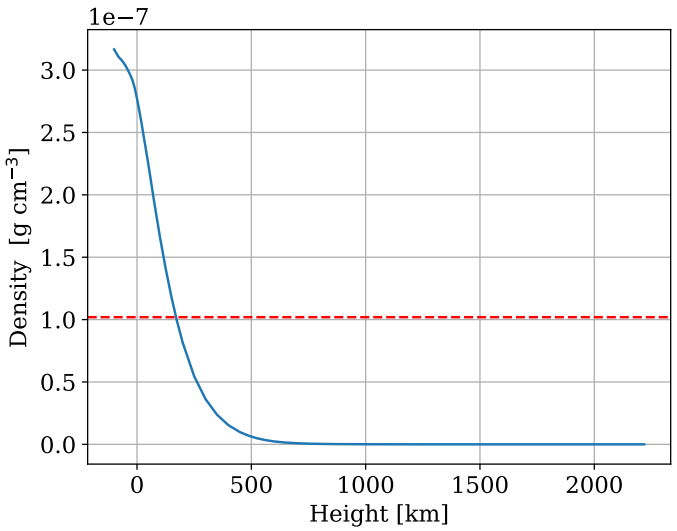

Fig. 6: The density plotted with respect to the height. We can see that the atmosphere is much denser deep in the photosphere until around 500 km from the surface. Here the density has decreased rapid and becomes quite constant. The density can be approximated by $\rho \approx \rho(0)\exp(-h/H_\rho)$, where H_ρ is the density scale height. The density scale height gives the height in the atmosphere over which the density fall by a factor of $1/e$. The scale height is marked by the red line in the figure. By studying the crossing point between the two lines, we can find the scale height $H_P = 170$ km.

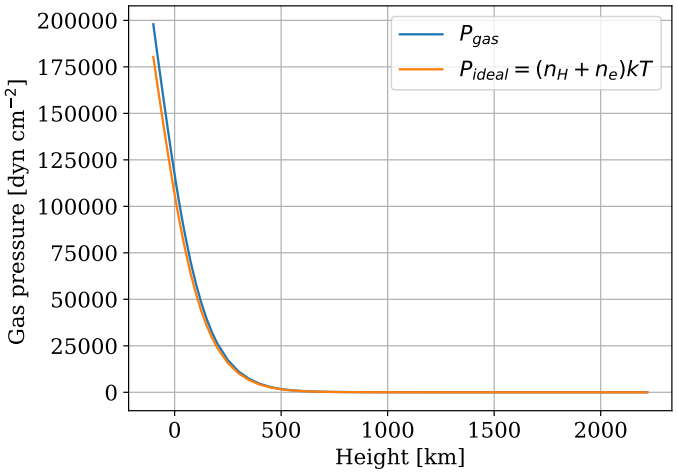

Fig. 7: Gas pressure and ideal gas pressure assuming we only have hydrogen and electrons plotted with respect to height.

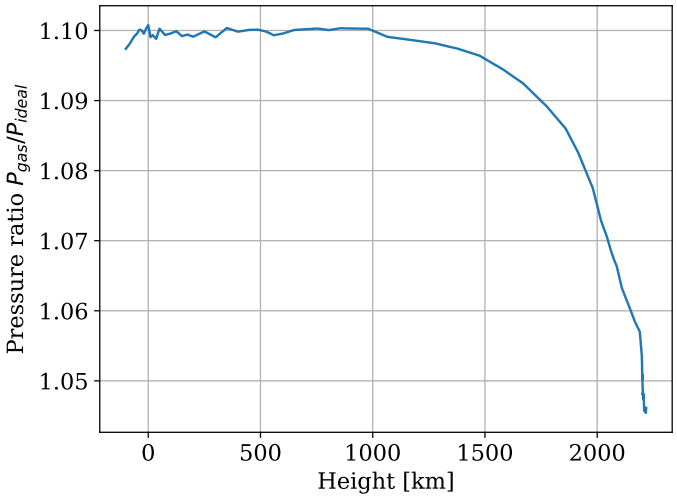

Fig. 8: The ratio between the gas pressure P_{gas} and the ideal gas pressure given by $P_{\text{ideal}} = (n_H + n_e)kT$ with only hydrogen and electrons, plotted against height. If they were the same, the ratio had been constant equal to one. We can see that the difference is largest in the at the surface of the Sun, but decreases further out.

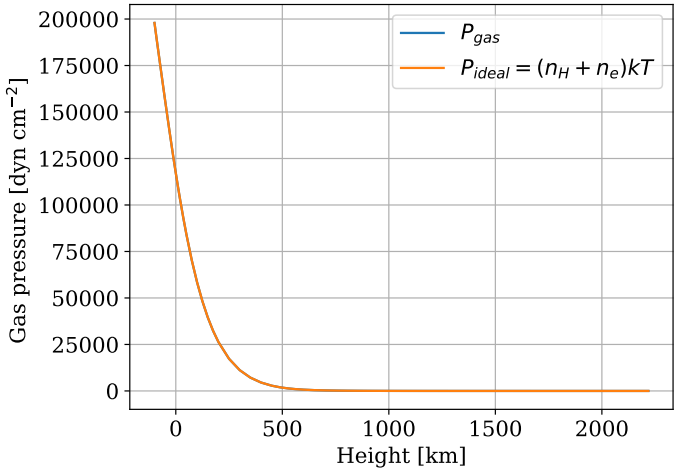

Fig. 9: Gas pressure plotted with respect to height. Also the ideal gas pressure is plotted, but now we have assumed that we have hydrogen, helium and electrons, and can see that the two graphs are more similar.

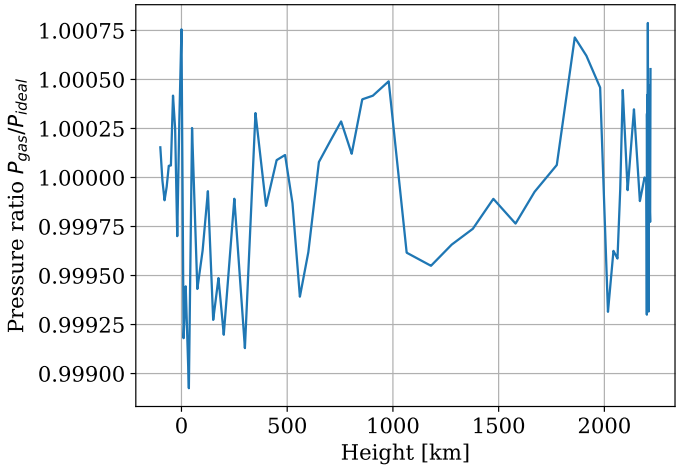

Fig. 10: The ratio between the gas pressure P_{gas} and the ideal gas pressure given by $P_{\text{ideal}} = (n_H + n_e + n_{He})kT$ with hydrogen, helium and electrons, plotted against height. Now we can see that the ratio oscillates around 1 on only very small scales. This might only be caused by uncertainty in the measured data or in the numerical calculations. So for this case we can safely assume that we have an ideal gas.

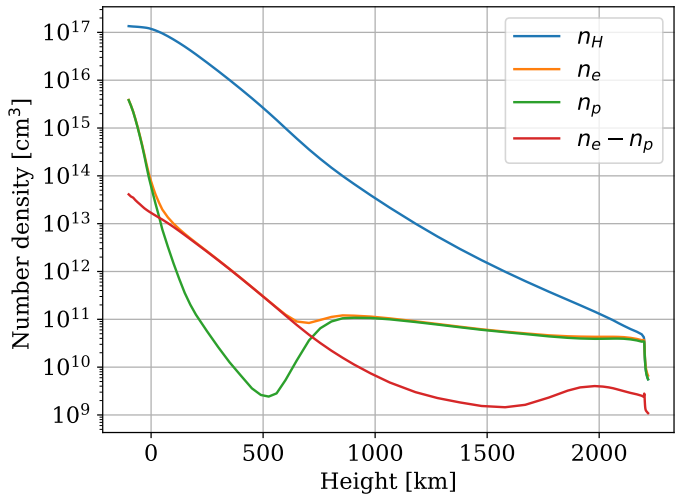

Fig. 11: The number density of hydrogen n_H, electrons n_e, protons n_e and electrons that do not come from hydrogen ionization $n_e - n_p$. We can see that all the number densities are highest at the surface of the star and decreases further out in the atmosphere as we would expect from the decreasing column mass in figure 5. Note that the number density of hydrogen and the number densiity of electrons that do not come from hydrogen ionization $n_e - n_p$ are parallel over a considerable height range. When we reach the transition region, the temperatures increases rapidly, making hydrogen begin to ionize. This causes the deviation of the two curves at the highest layers of the atmosphere.

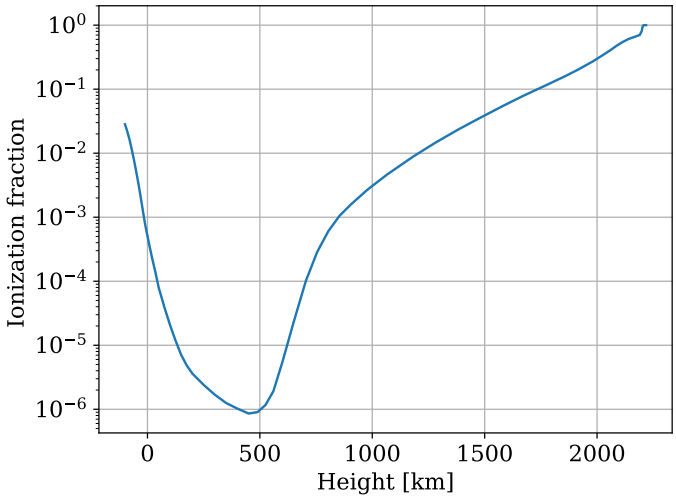

Fig. 12: The ionization fraction of hydrogen plotted with respect to height. We can see that it has a very similar shape to the temperature plot in figure 1. This reason for this, is that the ionization is strongly correlated with temperature. Higher temperature, means more energy, and therefore more ionized hydrogen.

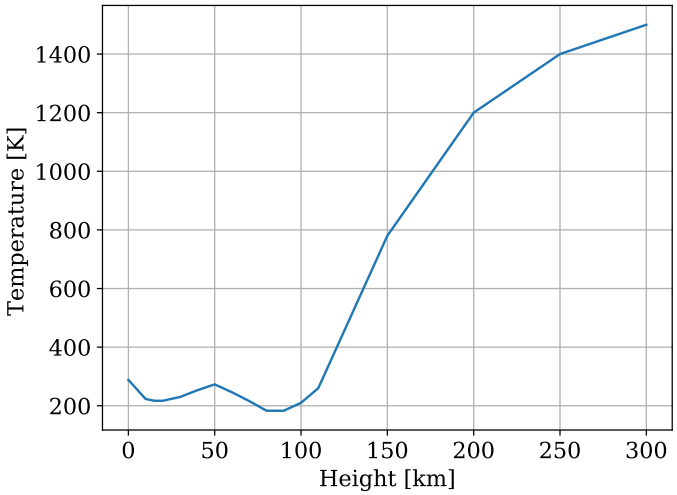

Fig. 13: The temperature of the Earth's atmosphere plotted with respect to height. We can see that similar to the solar atmosphere, the temperature in Earth's atmosphere increases further out.

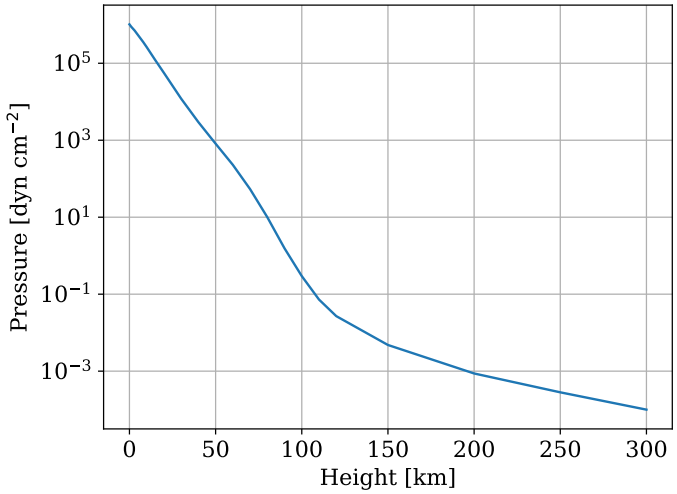

Fig. 14: The pressure of the Earth's atmosphere plotted with respect to height.

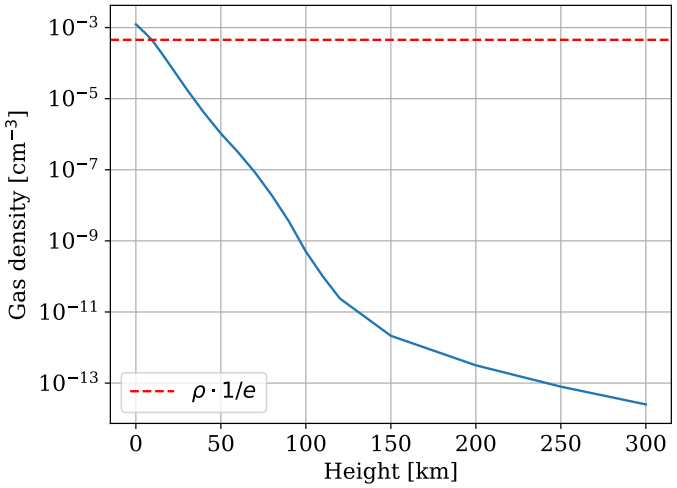

Fig. 15: The gas density of the Earth's atmosphere plotted with respect to height. The red line markes where the density has decreased with a factor of $1/e$, which defines the scale height. By studying the crossing point between the two lines, we can find the scale height $H_P = 9.3$. The pressure at Mount Everest is therefore $1/e \approx 0.35$ times the pressure at sea level. From figure 6, we found that the solar scale height was $H_p^{\odot} = 170$km, which is much larger than for the Earth.

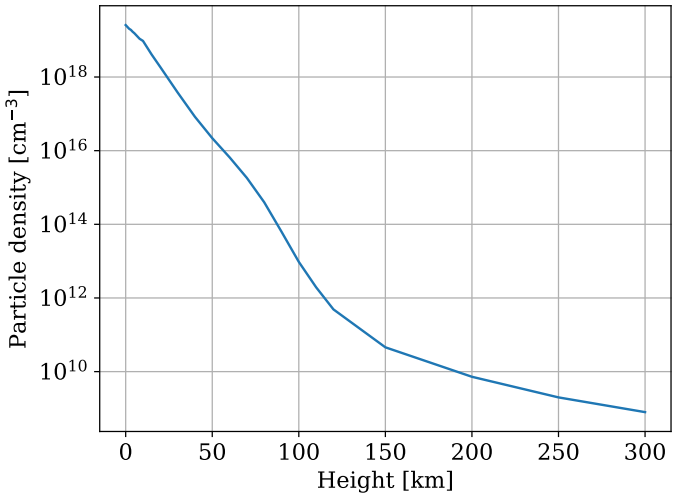

Fig. 16: The particle density of the Earth's atmosphere plotted with respect to height.

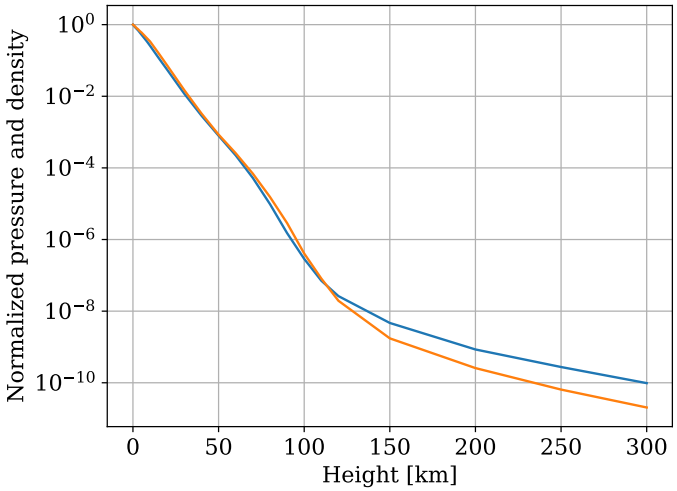

Fig. 17: Normalized pressure and density of Earth's atmosphere plotted with respect to height. We can see that they are very similar, which might indicate that the atmosphere can be assumed to be an ideal gas.

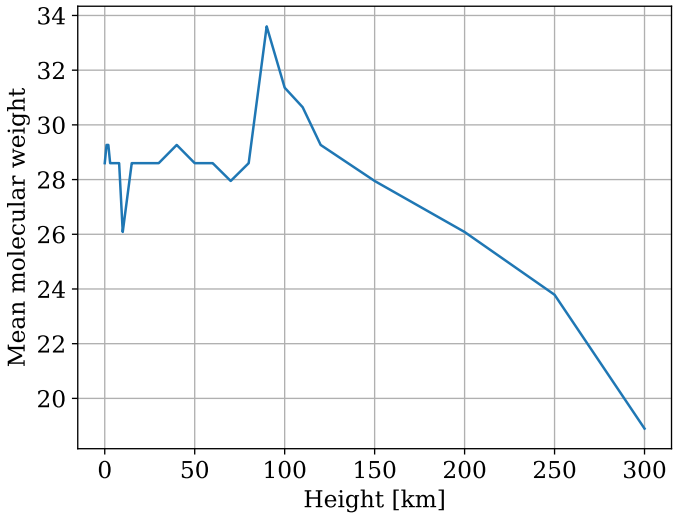

Fig. 18: Mean molecular weight $\mu_E \equiv \bar{m}/m_H = \rho/(Nm_H)$ plotted with respect to height. We can see that the mean molecular weight decreases higher up in the atmosphere. This is because the lightest elements (mainly helium and hydrogen) will dominate highest in the atmosphere, while the heavier elements as oxygen and nitrogen will dominate lower in the atmosphere.